Self-Assembly of Segmented Anisotropic Particles: Tuning Compositional Anisotropy To Form Vertical or Horizontal Arrays

Benjamin D. Smith, David J. Kirby, Isamar Ortiz Rivera, and Christine D. Keating*

Department of Chemistry, The Pennsylvania State University, University Park, Pennsylvania 16802, United States

ABSTRACT Columnar arrays of anisotropic nano- and microparticles, in which the long axes of the particles are oriented perpendicular to the substrate, are of interest for photovoltaics and other applications. Array assembly typically requires applied electric or magnetic fields and/or controlled drying, which are challenging over large areas. Here, we describe a scalable approach to self-assemble multicomponent nanowires into columnar arrays. Self-assembly of partially etched nanowires (PENs) occurred spontaneously during sedimentation from suspension, without drying or applied fields. PENs, which have segments that are either gold or "empty" (solvent-filled) surrounded by a silica shell, were produced from striped metal nanowires by first coating with silica and then removing sacrificial segments by acid etching. Electrostatic repulsion between the particles was necessary for array assembly; however, details of PEN surface chemistry were relatively unimportant. The aspect ratio and relative center of mass (COM) of the PENs were important for determining whether the PEN long axes were vertically or horizontally aligned with respect to the underlying substrate. Arrays with predominantly vertically aligned particles were achieved for PENs with a large offset in COM relative to the geometric center, while other types of PENs formed horizontal arrays. Assemblies were formed over >10 cm^2 areas, with over 60% of particles standing. We assessed array uniformity and reproducibility by imaging many positions within each sample and performing multiple assemblies of differently segmented PENs. This work demonstrates the versatility of gravity-driven PEN array assembly and provides a framework for designing other anisotropic particle systems that self-assemble into columnar arrays.

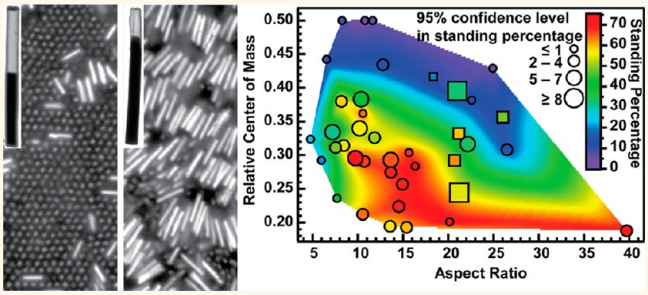

KEYWORDS: nanotube · aspect ratio · center of mass · nanowire · density · van der Waals · gold

Vertically oriented arrays of anisotropic micro- and nanomaterials[1] present an attractive combination of large surface area, high aspect ratio, and material properties. Within a solar cell, for example, recombination is minimized as the long axis effectively absorbs light, while the small axis quickly separates excitons.[2−4] Mechanisms for assembling columnar arrays from suspensions of anisotropic particles include alignment in applied electric or magnetic fields,[5−19] capillary forces during controlled sample drying,[20−31] solvation/depletion effects,[32−39] and templating.[40−45] In a few cases, approaches based on drying methods or electric fields have yielded large-area arrays (>1 cm^2).[10,30] Obtaining orientational fidelity in structures of these sizes generally required high levels of control over the particle sizes, substrates, and experimental conditions; though recent work showed assembly over a 1 cm^2 area with less stringent considerations.[15,28] Despite numerous assembly methods reported for single-component nanorods, the assembly and orientation of multisegmented nanomaterials, desirable in nanoelectronics and other applications, is extremely rare. Arrays in which multisegmented particles are oriented the same direction have been produced after assembly by reactions that occur preferentially at the top of the array to produce the segments.[16,17,27] In nearly every case of columnar self-assembly, the small size of the individual nanoparticles (typical reports feature CdS or CdSe nanorods with diameters of 1−10 nm and lengths of 10−30 nm) necessitated sample drying prior to characterization (*e.g.*, by SEM).

* Address correspondence to keating@chem.psu.edu.

Received for review November 20, 2012 and accepted December 17, 2012.

Published online December 17, 2012
10.1021/nn305394s

Columnar arrays with much larger individual component sizes (*i.e.*, micrometer-long wires) are of interest for some applications; these are typically produced by top-down methods. For example, high-quality photovoltaic arrays have been produced in-place using directed growth methods.[46−48] When micrometers-long nanowires are allowed to self-assemble, they typically lay down with their long axis parallel to the underlying substrate. For example, Au nanowires of either 2 or 4 μm length form horizontal smectic assemblies.[49] Applied magnetic or electric fields have been used to orient particles perpendicular to the substrate,[5,6,14] but these methods do not produce closely packed, high-density arrays. High-density three-dimensional structures have been achieved for polymer/metal segmented nanowires through a combination of templating and capillary forces.[40−43] These structures can form curved superstructures that would be difficult or impossible to produce by other means but are less amenable to forming large-area planar arrays. We recently reported a gravity-driven approach to self-assemble multicomponent particles from suspension in the absence of templating, capillary forces, or applied fields.[50] Unlike the applied electric or magnetic fields used in other studies, the gravitational field is both ubiquitous and highly uniform. Partially etched nanowires (PENs) in which a thin silica shell surrounded a cylindrical core half filled with gold assembled to form columnar arrays with the denser Au-filled ends faced down and the lighter, solvent-filled ends facing up. Vertical particle orientations were achieved by oriented initial impact and rotation from initially horizontal orientations, with columnar arrays observed for high surface coverages of PENs. The less dense solvent-filled segment clearly assisted vertical PEN orientations, serving as a sort of "assembly handle". Whether, and to what extent, this assembly mechanism could be generalized was unclear since only half-Au/half-empty PENs in deionized water had been evaluated.[50]

Here, we explore the generality of gravity-driven PEN self-assembly by varying particle and solution characteristics. Forty different classes of PENs were prepared and assembled, which enabled us to map out the effects of PEN composition. Figure 1a illustrates the basic PEN geometry and gives the ranges explored for each PEN dimension. Particle coatings and solution ionic strength were also varied to determine their affect on assembly. We found the particle-driven, gravity-induced PEN assembly strategy to be a versatile route for production of vertically or horizontally aligned arrays of anisotropic particles, compatible with assembly over large areas (>10 cm^2).

RESULTS AND DISCUSSION

PENs were prepared from Au/Ag striped metal nanowires synthesized by electrodeposition in porous alumina templates.[50−54] After release from the template, the nanowires were silica-coated and Ag segments were subsequently removed by nitric acid etch.[50,55] The resulting PENs had porous silica shells the size and shape of the original nanowires but were only partially filled by the remaining Au core segments (Figure 1a). Throughout the article, PEN patterns are described as *x*Au-*y*E, where *x* and *y* are the length in micrometers of each segment. For example, 2Au-2E indicates a silica-coated particle in which the core is 2 μm of Au followed by 2 μm of etched region (Figure 1a). Each batch of PENs was characterized by transmission electron microscopy (TEM) to determine dimensions of the Au core, etched regions, and silica shell as well as the overall particle length and diameter. This information can be found in Supporting Tables 1−4. Because in earlier work the particle concentration was an important variable,[50] for each of the experiments described here, the particle concentration was matched to the assembly area such that enough PENs were present to fully cover the surface if they formed a vertically oriented monolayer (*e.g.*, 1−2 × 10^9 PENs/mL for most experiments; see Experimental Section).

PEN Composition. We began by varying length, number, and position of Au core segments within PENs of constant overall dimensions (4 μm length and 290 nm cross-sectional diameter). Because the Au cores are primarily responsible for both the overall mass of individual PENs and van der Waals attractions between them, changes in the amount and location of Au core segments were expected to impact assembly. We describe core arrangements in terms of PEN center of mass (COM), which is reported as the fractional offset from the more dense end of the particle. For symmetric PENs (*e.g.*, solid Au cores) COM = 0.5 and for 1Au-3E PENs, COM = 0.213, as illustrated in Figure 1a. Aqueous PEN suspensions were placed into sealed chambers atop glass coverslips for assembly and observed from below using reflectance optical microscopy. Hence, for PENs in horizontal orientations, Au cores appear as bright rods while "empty" solvent-filled silica tube regions appear dark. Vertically oriented PENs appear as a bright dot.[50] Images of individual particles and corresponding assemblies for a range of COMs are shown in Figure 2.

The PENs in panels a, e, and f had COMs of 0.5 and formed horizontal arrays, with less than 10% of particles oriented vertically. 2Au-2E PENs, however, had a COM of 0.275 and showed standing of 68%, consistent with our earlier work on this specific PEN pattern.[50] We observed areas of all vertically aligned particles that are approximately 50 to 400 μm^2 in size interspersed with horizontally oriented PENs. Primarily vertical assemblies also resulted for PENs with COM 0.21 (Figure 2d). The relative amount of Au core to solvent-filled shell regions was much less important than the position of these regions, which dictated whether and by how much the particle COM was offset from the center.

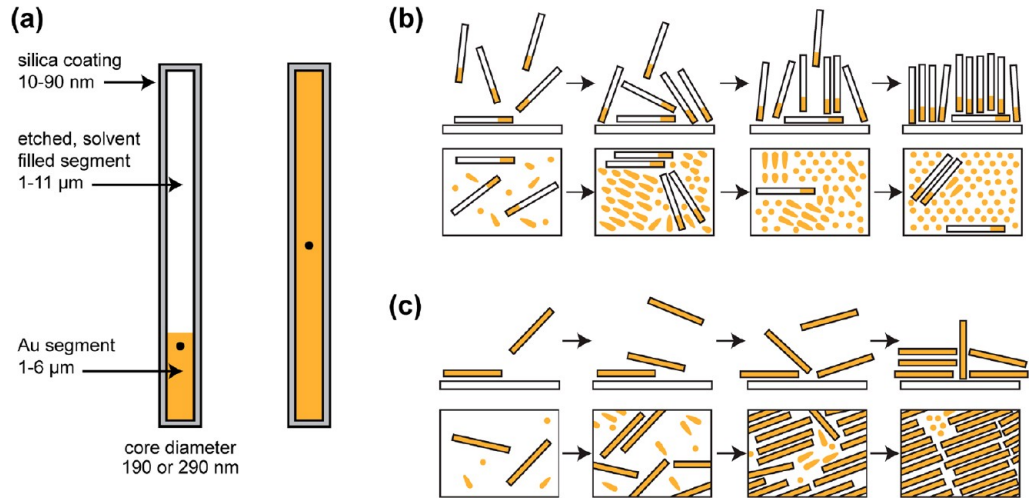

Figure 1. General form of a partially etched nanowire (PEN) and depiction of the center of mass (COM). (a) PEN comprises Au segment(s) and an etched, solvent-filled segment, contained within an amorphous SiO_2 shell. Within the ranges shown, the lengths of each segment, the diameter of the PEN, and the glass thickness were adjusted. The ratio, size, and number of Au and etched segments determined the COM of the particle. Examples of 4Au (a 4 μm Au PEN) and 1Au-3E PENs (a PEN with 1 μm Au and 3 μm etched segments) are shown here, with their respective COMs represented as black dots. The relative COMs are 0.5 and 0.213 for the 4Au and 1Au-3E PENs, respectively. The self-assembly behavior over time of 1Au-3E (b) and 4Au (c) is illustrated. These illustrations depict assembly from both a side (above) and bottom (below) view. As time passes, the PENs sediment, accumulating on the surface. With sufficiently high surface concentrations, the 1Au-3E PENs form vertically aligned arrays, while the 4Au PENs form smectic rows.

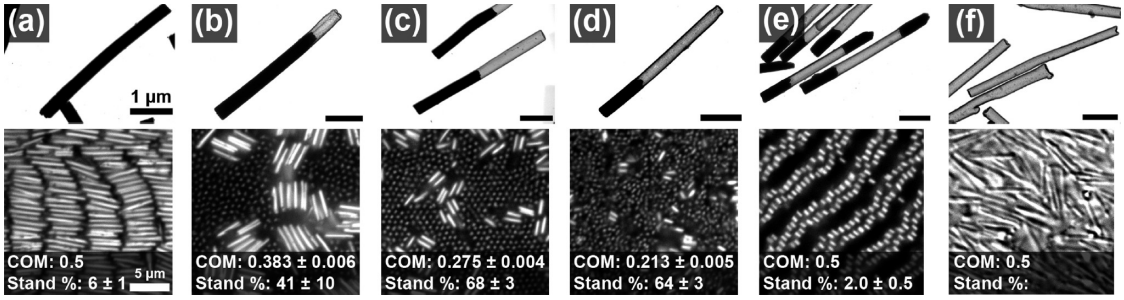

Figure 2. Partially etched nanowires (PENs) and their self-assemblies. Transmission electron micrographs of PENs, all approximately 4 μm in length and 290 nm in diameter, including (a) 4Au; (b) 3Au-1E; (c) 2Au-2E; (d) 1Au-3E; (e) 1Au-2E-1Au; and (f) 4E. The electron-dense Au appears black, while the silica coating is gray. Optical microscope images of self-assembled arrays are shown below: (a–e) bright-field reflectance—Au appears bright; (f) transmitted light (differential interference contrast). All of the PENs and arrays shown are typical of those in a given sample. The micrographs were obtained *via* inverted microscopy; hence the bottom of the sample is visualized. The center of mass and average standing percentage for each wire set is listed, except for (f), which was too disordered to count effectively.

This can be seen by comparing the assemblies of Figure 2c,e, which have the same amount of total Au and empty regions but differ greatly in COM and standing percentages (68% standing for COM 0.27 and 2% for COM 0.5). For 3Au-1E PENs, which have COM = 0.38, intermediate values of standing percentage were observed (41%), with heterogeneity across the sample. Near the edge of the assembly chamber, 3Au-1E PENs showed high standing values, >60% (Supporting Figure 1) due to the hydrophobic spacer influencing assembly behavior,[49] while in the central regions, more PENs had a horizontal orientation.

The PEN assembly process is depicted for COM = 0.2 and 0.5 in Figure 1b,c. During sedimentation, PENs impacted the surface with near-vertical orientations, after which they fell into horizontal orientations at low surface coverage. For PENs with offset COM, the denser end impacted first and remained on the surface when PENs that had lain down rotated up away from the underlying surface. At higher surface coverage, these PENs adopted vertical orientations supported by neighboring particles. In contrast, particles with COM = 0.5 formed horizontal assemblies even at high surface coverages. Supporting Figures 2 and 3 describe this assembly process for 2Au-4E and 5Au-2E PENs, which was similar to that reported previously for 2Au-2E PENs.[50] Supporting Figure 4 shows the specific numbers of particles oriented either vertically or horizontally over time. As previously observed,[50] the number of horizontally oriented PENs increases and then slightly decreases, indicating their conversion between orientations. Although counterintuitive, the transition from a horizontal to vertical orientation is an important part of the assembly mechanism and can be observed

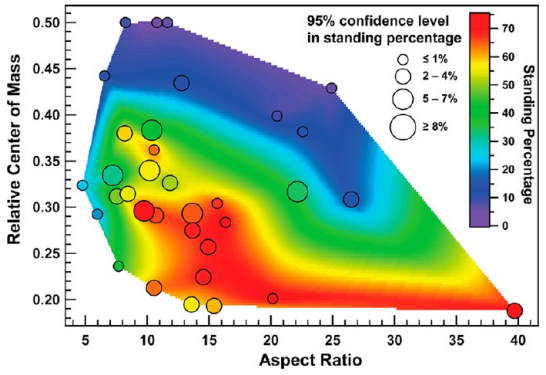

Figure 3. Plot showing the standing percentages for filled and partially etched nanowire samples with varying aspect ratios and relative centers of mass. The circles each indicate a series of experimental sets from which the colored surface was interpolated. The color of each circle indicates average standing percentage, while the size signifies the 95% confidence interval. All measured and calculated values, with associated confidence intervals for these PEN sets, can be found in Supporting Tables 1 and 2.

in movies taken during the process.[50] Assembly occurs over approximately 15 min and depends on the sedimentation rate of the given PEN set since high surface concentrations are needed to induce vertical orientation of the PENs.[50]

Effect of Aspect Ratio and Center of Mass. Variations in segment length, material, and number were used to further examine the relationship between standing percentage and particle characteristics. Thirty-three different sets of PENs, with a nominal diameter of 290 nm, were prepared to have aspect ratios (ARs) between 5 and 40 and COMs from 0.19 to 0.5. Higher AR PENs were susceptible to bending and breakage (for instance, the 2Au-11E PENs AR = 39.7, COM = 0.188 had substantially more broken and bent wires),[52] while shorter PENs (specifically those with Au lengths <1 μm) were difficult to analyze *in situ*. Full particle characteristics are found in Supporting Tables 1 and 2. Figure 3 plots standing percentage as it depends on the relative COM and AR. Red indicates regions of close-packed, vertically aligned domains, while violet areas had larger smectic or disordered particle domains aligned parallel to the substrate. Since the background heat map is interpolated, it should be only be used to guide the eye, especially when far between experimental values. The best columnar assemblies, with >60% standing, were obtained for PENs with an aspect ratio of 10 to 20 and a center of mass that was offset by at least 20% of the total length, though at least 50% standing was observed for a much wider range. The highest observed standing percentage was limited to 72% averaged over an entire set of arrays. Perfect vertically aligned regions of 50 to 400 μm^2 were common in these arrays. In the image shown in Supporting Figure 5a, a standing percentage of 84% was determined; we observe numerous areas such as this one in our assemblies. We believe limits on the overall standing percentage of the array were due to multilayer formation (Supporting Figure 6) inhibiting further conversion of PENs to vertical orientations and broken/aggregated particles. We note that many of these multilayered particles appear vertically oriented. Overall, we observed an inverse relationship between the COM of a PEN set and the resulting standing percentage but no clear relationship between AR and standing percentage (Supporting Figure 7). PENs with the largest ARs, and thus long lengths, were observed to interweave as large numbers deposited, creating disordered arrays (Supporting Figure 1b). PENs with large ARs and very low COMs, however, still oriented vertically.

Smaller Diameter PENs. Because not only COM and AR but also total particle mass, van der Waals attractions, sedimentation, and diffusion rates, *etc.* impact assembly, it was not clear whether the trends observed in Figure 3 would be instructive for assembly of other particles. Therefore, we also tested PEN sets with diameters of approximately 190 nm for a range of COM values. These smaller diameter PENs have reduced overall mass, which impacts sedimentation and diffusion rates as well as van der Waals attractions. Assemblies of the 190 nm diameter PENs behaved similarly to their larger diameter analogues, with higher standing percentages for greater offsets in COM (Figure 4). We generally observed higher standing percentages for these PENs than expected for a similar PEN with a larger diameter, which could be a result of the enhanced diffusion, lower mass, *etc.* of these smaller particles (Supporting Figure 8 plots the standing percentages onto Figure 3 for comparison). The general trends, and the important role of COM for columnar assembly, remained applicable for these PENs.

Consequences of an Offset COM. The offset COM of a PEN, which resulted from having a large etched segment and a small Au segment, affected both the self-assembly process and interparticle interactions. PENs with lower COMs oriented more vertically both during deposition and after reaching the surface. Supporting Figure 10 shows the orientation distribution of PENs during impact. PENs with a lower COM also exhibited greater rotation off the substrate plane, which is important because it provides a mechanism for conversion from horizontal to vertical orientations after depositing on the surface (see Figure 1b, ref 50, and Supporting Figure 4). PENs with COM values <0.35 showed a decrease in the number of "laying" wires over time during assembly, while higher COM PENs acted similar to previously studied all-Au nanowires showing alignment parallel to the surface.[49]

We hypothesize that the standing orientation may provide a route to maximizing van der Waals interactions between the PENs' Au cores. A vertically oriented assembly orients the Au segments with respect to those on neighboring particles more effectively than

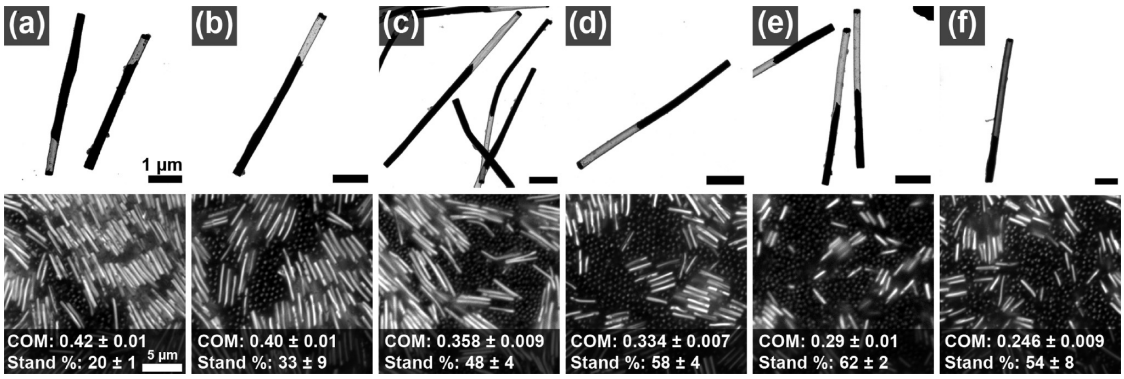

Figure 4. Partially etched nanowires (PENs) and their self-assemblies. Transmission electron micrographs of PENs, all approximately 190 nm in diameter, including (a) 3.5Au-1E; (b) 3Au-1E; (c) 4Au-2E; (d) 3Au-2E; (e) 2Au-2E; and (f) 2Au-4E. The electron-dense Au appears black, while the silica coating is gray. Optical microscope images of self-assembled arrays are shown below. All of the PENs and arrays shown are typical of those in a given sample. The micrographs were obtained *via* inverted microscopy; hence the bottom of the sample is visualized. Au appears bright in these reflectance images. The center of mass and average standing percentage for each PEN set are listed. Supporting Figure 9 shows the distribution of diameters of the particle sets with full measurements found in Supporting Table 3.

is likely in horizontal arrangements since the hollow silica segments in PENs may prevent favorable van der Waals interactions. We note that the hollow silica segment should be solvent-filled and is not more buoyant than the surrounding media. In horizontally oriented smectic arrays, which are seen for all-Au wires (COM 0.5), neighboring wires maximize attractive van der Waals interactions along the entire wire length.[49] Here we observed 4Au and 1Au-2E-1Au PENs forming smectic rows where the Au segments are aligned (Figure 2a,e). Completely etched tubes, 4E PENs, had no metallic cores and therefore weak van der Waals attractions. These tubes produced only disordered multilayered arrays instead of either smectic rows or columnar arrays (Figure 2f).

Assembly Chamber Size. Since no external applied fields or controlled drying is needed, this assembly strategy should be amenable to larger areas, relatively independent of area. To test this, assembly chambers defined by silicone spacers of three different sizes, 0.01, 0.64, and 10.8 cm^2 (Supporting Figure 11), were used to examine scalability of arrays of 2Au-2E PENs (Supporting Table 4). To our knowledge, the >10 cm^2 area assembled here is the largest example of a self-assembled columnar structure achieved, though highly oriented assemblies have been produced on the 1 cm^2 scale.[10,30] As can be seen in Figure 5, these assemblies displayed similar behavior. The micrographs from each sample did not differ qualitatively between samples; assemblies of vertically oriented PENs had horizontally aligned trapped (or malformed) PENs interspersed. Quantitatively, they were similar as well with standing percentages increasing over time, reaching over 65% standing. Supporting Figure 12 displays histograms of standing percentages for many regions in these samples, and Supporting Figure 5 shows a subset of the images from which histograms were generated. A composite image generated from

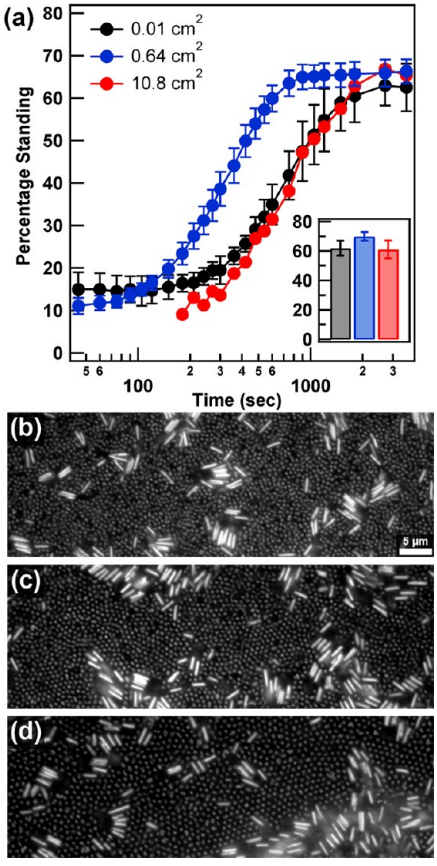

Figure 5. Partially etched nanowires (PENs) assembled on substrates of different sizes. (a) Plot of the standing percentage of assemblies completed within small (black, 0.01 cm^2), medium (blue, 0.64 cm^2), and large (red, 10.8 cm^2) chambers over time. The difference in the onset of increasing standing percentage is due to the difference in spacer height and thus nanowire deposition time. The inset shows the average standing across these assemblies after 1 h has elapsed. Representative reflectance micrographs for chambers of (b) 0.01, (c) 0.64, and (d) 10.8 cm^2 are shown.

six adjacent images shows a larger, contiguous area (Supporting Figure 13). As mentioned above for the

3Au-1E PENs (Supporting Figure 1), we observed edge effects near the silicone spacers used to define the sample volume. Otherwise, arrays were generally quite homogeneous, as shown by the histograms in Supporting Figure 12, with the exception of the aforementioned 3Au-1E PENs. For a PEN set that stands, the assembly mechanism is driven by the surface concentration and gravity.[50] Therefore, the resulting columnar structures should be scalable to any substrate size.

Electrostatic Contribution to Self-Assembly. All of the assembly experiments described above were performed in DI H_2O. To explore the importance of electrostatic repulsion within gravity-driven PEN assembly, we varied the solution ionic strength and PEN surface chemistry. The SiO_2 coating on the PENs carries a negative charge.[50,56] Literature values for the zeta-potential of silica nanospheres prepared by similar sol−gel methods range from −20 to −30 mV in water with a similar pH to that used here.[57,58] We observed 2Au-2E PENs (Supporting Table 4) within NaCl solutions to examine the stability of the assemblies as the Debye screening length, κ^{-1}, decreased. In a 100 μM NaCl solution (κ^{-1} = 28 nm), identical behavior to those in deionized water (κ^{-1} = 68 nm, pH approximately 4.7)[49] was observed (Figure 6a,b). In a 1 mM NaCl solution (κ^{-1} = 9.6 nm), however, the standing percentage decreased and clumps of particles appeared (Figure 6c). These clumps decreased the vertical alignment from >60 to about 40% by creating more areas of off-axis assembly (*i.e.*, leaning particles). With 100 mM NaCl (κ^{-1} = 1 nm), instant aggregation between PENs was observed within the sample (Figure 6d). These results match earlier work for horizontally aligned all-Au particles, which formed smectic arrays with several different electrostatically repulsive coatings.[49] Electrostatic repulsions ensure that the particles do not aggregate, thereby allowing assembly to occur. The silica coating therefore both preserved the pre-etched nanowire shape and imparted an overall negative surface charge through deprotonated −OH groups, which stabilized the particles and their arrays.[50,56]

Many surface chemistries could provide an electrostatic repulsion and retain the particle shape. We examined both polyelectrolyte coatings and modified silicas on 2Au-2E PENs as example systems of alternate functional coatings. Polyelectrolytes have been used to incorporate drugs and enzymes into coatings, while the modified silicas have prevented biofouling and selectively sequestered ions.[59−64] Supporting Figure 14 shows representative micrographs from assemblies of polyelectrolyte-coated PENs onto similarly coated and uncoated surfaces. PENs prepared with organically modified silicas coatings, silicas with functional groups incorporated throughout,[62] also showed columnar assemblies (Supporting Figure 15). While the self-assembly process depended on the heterogeneous internal composition of the PENs, the process appeared independent of coating as long as charge repulsion remained.

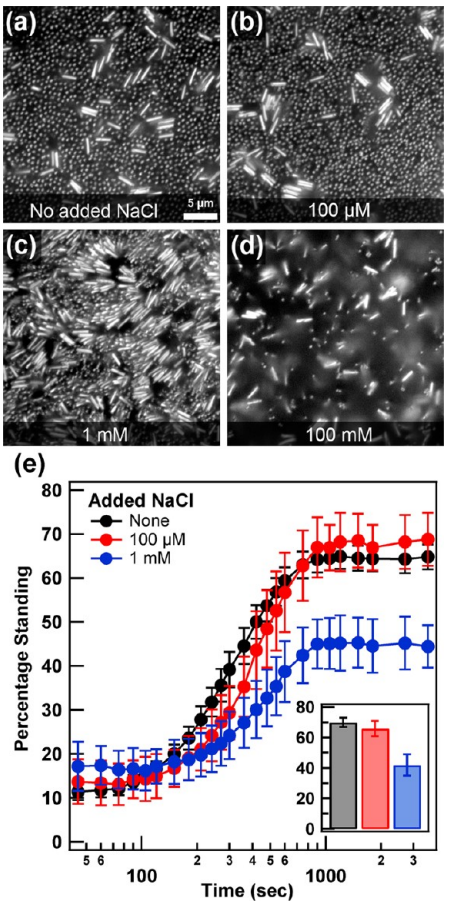

Figure 6. Partially etched nanowire (PEN) assembly completed in different NaCl solutions of various concentrations. (a−d) Representative reflectance micrographs for nanowire suspensions. The PENs in (d) immediately froze into position upon contacting the surface/other nanoparticles, hence the large open framework seen. This structure still included many perpendicularly aligned nanowires. (e) Plot of assembly over time for three concentrations of added NaCl. Inset shows the average standing across many samples for the same salt additions after 1 h had elapsed.

Overall Assembly Mechanism. We observe three important forces at work in this system: electrostatic repulsion, gravity, and van der Waals attraction. Electrostatic repulsion is necessary to prevent the particles from aggregating or sticking to the substrate; assembly is possible only when the particles do not aggregate first. Gravity sediments the particles to create high surface densities and orients them as they fall. High surface densities are needed in order to stabilize vertical orientations of the particles.[50] Once enough particles are on the surface and standing is stabilized, particles which subsequently fall to the surface in a vertical orientation probably retain this orientation. At early times when PEN surface coverage is low, gravity does not provide a driving force for vertical orientation. After impact, particles lay down on the surface. These initially horizontal PENs sample vertical orientations and

ultimately convert to vertical orientations driven, we hypothesize, by van der Waals attractions particularly between the Au core segments.

The etched segments of PENs are not expected to contribute much toward overall van der Waals attractions since the Au Hamaker constant is at least an order of magnitude greater than for any other material used here.[65,66] The system, therefore, produces the most energetically favorable array when these Au cores are aligned. In order to maximize attractions, PENs with large etched segments (therefore, those with highly shifted COMs) must align the Au core segments on neighboring PENs. Since gravity necessitates that the dense Au core remains on the surface, all vertically oriented particles have their cores automatically aligned and have the opportunity for more nearest-neighbors (six, in hexagonal vertical arrays). Particles arrayed parallel to the surface, however, would have fewer nearest-neighbors due to the presence of the underlying silica substrate. They are also more likely to be trapped in unfavorable alignments since 180° rotations would be needed to sample PEN orientations; such rotations are inhibited by the presence of other particles both within the plane and above it (the latter when multilayers form). Hence, optimized PEN−PEN interactions are facilitated by vertical orientations, and columnar arrays result from a balance of electrostatics, gravitational concentration/orientation, and these asymmetric van der Waals attractions.

CONCLUSIONS

Spontaneous, gravity-driven self-assembly of partially etched nanowires into columnar arrays in the absence of applied external fields and/or drying forces was observed over a wide range of conditions. By adjusting the relative center of mass, assemblies with primarily horizontal or vertical PEN alignments were achieved. Vertically aligned arrays are of particular interest because they are difficult to achieve by self-assembly methods in the absence of external applied fields; the offset center of mass approach developed here provides a means of achieving such arrays. PENs with an aspect ratio from 10 to 20 and a COM under 0.3 displayed the best columnar structures, with PEN standing percentages >60%. Arrays were formed over >10 cm^2 areas with more than 60% of the nanowires vertically aligned. Electrostatic repulsion was necessary to prevent aggregation and allow assembly; otherwise, the specific coating (polyelectrolyte, modified and unmodified silica) did not affect assembly. Efforts are underway to increase the standing percentages, which are limited by multilayers and imperfect particles. It is of interest to expand the materials (both internal segments and coatings) and particle sizes to further elucidate the assembly process and ultimately facilitate assembly of device-applicable structures.

The role played by solvent-filled silica shell regions should be a rather generic one; that is, other materials with much lower density and sufficient van der Waals interactions may serve a similar function. Low-density "assembly handles" such as the solvent-filled silica shell regions employed here may provide a means for assembly of multicomponent anisotropic particles into vertically aligned arrays without the use of applied electric or magnetic fields or drying forces.

EXPERIMENTAL SECTION

Materials. All water used in these experiments was purified to >18.2 MΩ·cm, using a Barnstead Nanopure filtration system, or was BDH Aristar Plus HPLC grade water (low TOC) from VWR. Alumina membranes, with a nominal pore diameter of 0.2 or 0.02 μm, were purchased from Whatman. Orotemp 24 and Silver Cyless R plating solutions were purchased from Technic Inc. Tetraethoxysilane (TEOS), 3-aminopropyltrimethoxysilane (APTMS), and the organically modified silanes were purchased from Gelest. CoverWell perfusion chamber gaskets were purchased from Invitrogen, or spacers were cut from a large piece of silicone from Allstate Gasket and Packing. Large coverslips, 4.5 × 6.25 in., were purchased from Brain Research Laboratories. Polyallylamine hydrochloride (PAH) and sodium polystyrene sulfonate (PSS) were purchased from Sigma. All chemicals were used as received except where noted.

Nanowire Preparation. Nanowires were grown by electrochemical deposition in the pores of alumina membranes following previously reported methods.[51−54] Briefly, silver was coated onto one side of a membrane *via* metal evaporation to serve as a working electrode. Materials were then plated under a constant current with the length of each metal segment controlled by the deposition time. After dissolution of the backing electrode layer and membrane, the nanowires were coated with silica and selectively etched, as described elsewhere.[50,55]

Nanowire Assembly. As described previously,[49,50] a silicone spacer was rinsed with water and placed onto a glass coverslip (typically 24 × 60 mm); this formed wells 9 mm in diameter and 2.5 mm deep. The smaller (0.12 cm diameter, 0.67 cm height) and larger chamber (4.11 × 2.61 cm, 0.67 cm height) were constructed from a large piece of silicone. All PENs were rinsed into deionized water prior to assembly. The chamber was allowed to rest on the microscope stage while the nanowires were added. On the basis of our previous work, in order to cover the surface with a vertically oriented monolayer, 1.8×10^8 PENs/cm^2 were needed.[50] For the 0.64 cm^2 spacer typically used, we used 100 μL of a $1-2 \times 10^9$ PENs/mL suspension. Here, concentration is given as a range since it was based the on average batch concentration, determined elsewhere.[50,55] Nanowire suspensions were sonicated immediately before addition to each well. A coverslip was then placed on top of the spacer to seal the well and prevent drying from affecting the assembly. All coverslips were rinsed with deionized water and dried before use.

Imaging. Optical microscopy was performed on a Nikon Eclipse TE300 or Nikon Eclipse TE200 inverted microscopes with either Xe or Hg lamps and Photometrics CoolSNAP HQ cameras. Plan Fluor and Plan Apo 100× oil objectives (NA 1.4 and 1.3, respectively) were used. Reflected bright-field images were taken using white light with Image Pro Plus (versions 4.5 or 7.0; Media Cybernetics). Transmission electron microscopy was performed on a JEOL JEM 1200 EXII. Images were collected at an operating voltage of 80 or 120 kV on a Tietz F224 camera.

Image Analysis. Images from which standing percentages were determined were processed using Image Pro Plus (version 7.0) as previously described.[50] Briefly, a filtered image

was counted for objects larger than 9 pixels. These objects were classified into two groups based on the ratio of the objects largest radius to its smallest radius; objects with a radius ratio smaller than 3 were classified as standing, while those with a ratio larger than 3 were determined to be lying down. We note that typically 10−20% of particles are identified as "standing" in early time points. This occurs for three reasons. First, some particles are simply vertically oriented. Second, many of the particles observed early are impacting the surface. Particles generally impact while oriented vertically. Third, our analysis results in some misidentification of particles (as compared to hand counts) at particle densities under $5-8 \times 10^7$ NWs/cm^2. We were primarily interested in indentifying particles in high-density arrays, where our identification is more error-free. In comparisons with hand counts, the overall total number of PENs determined was within ±5% of hand count at all time points. To characterize the arrays, images were collected in two ways. First, images were collected at specified time points, at a single location, for at least six separate experiments. Following that 1 h of observation, at least 20 images taken during manual rastering across the entire chamber were collected. These images reflected the overall assembly features. Successful experiments were defined as any assembly without broken, bundled, or clumped wires (no more than 1% of the observed PENs), or without any or observed aggregation or stickiness. For the large-area assembly (>10 cm^2), >500 images were taken across the whole surface in order to ensure a representative characterization of the assembly.

Nanowire dimensions were determined from transmission electron micrographs using NIH ImageJ software. For each sample at least 30, but usually >50, nanowires were examined. Measurements for each length, width, and thickness were taken at two places along the wires.

Conflict of Interest: The authors declare no competing financial interest.

Acknowledgment. Acknowledgment is made to the Donors of the American Chemical Society Petroleum Research Fund for primary support of this research (ACS PRF 50888-ND10). Additional support was from the Center for Materials, Structures, and Devices, one of six research centers funded under the Focus Center Research Program (FCRP), a Semiconductor Research Corporation entity. We appreciate the use of the Huck Institute of Life Sciences Electron Microscopy Facility. We thank Dr. S. Dean for coating PENs with organically modified silicas.

Supporting Information Available: Additional figures, tables, and methods as described in the text. Transmission electron micrographs, bright-field reflected micrographs, tables of measured nanowire dimensions and characteristics, and plots of standing percentage, measurement error, and measurement distributions. This material is available free of charge *via* the Internet at http://pubs.acs.org.

REFERENCES AND NOTES

1. Krahne, R.; Morello, G.; Figuerola, A.; George, C.; Deka, S.; Manna, L. Physical Properties of Elongated Inorganic Nanoparticles. *Phys. Rep.* **2011**, *501*, 75–221.
2. Hochbaum, A. I.; Yang, P. Semiconductor Nanowires for Energy Conversion. *Chem. Rev.* **2010**, *110*, 527–546.
3. Spurgeon, J. M.; Atwater, H. A.; Lewis, N. S. A Comparison between the Behavior of Nanorod Array and Planar Cd(Se,Te) Photoelectrodes. *J. Phys. Chem. C* **2008**, *112*, 6186–6193.
4. Law, M.; Greene, L. E.; Johnson, J. C.; Saykally, R.; Yang, P. Nanowire Dye-Sensitized Solar Cells. *Nat. Mater.* **2005**, *4*, 455–459.
5. Wang, J.; Scampicchio, M.; Laocharoensuk, R.; Valentini, F.; González-García, O.; Burdick, J. Magnetic Tuning of the Electrochemical Reactivity through Controlled Surface Orientation of Catalytic Nanowires. *J. Am. Chem. Soc.* **2006**, *128*, 4562–4563.
6. Loaiza, O. A.; Laocharoensuk, R.; Burdick, J.; Rodríguez, M. C.; Pingarron, J. M.; Pedrero, M.; Wang, J. Adaptive Orientation of Multifunctional Nanowires for Magnetic Control of Bioelectrocatalytic Processes. *Angew. Chem., Int. Ed.* **2007**, *46*, 1508–1511.
7. Zorn, M.; Tahir, M. N.; Bergmann, B.; Tremel, W.; Grigoriadis, C.; Floudas, G.; Zentel, R. Orientation and Dynamics of ZnO Nanorod Liquid Crystals in Electric Fields. *Macromol. Rapid Commun.* **2010**, *31*, 1101–1107.
8. Gupta, S.; Zhang, Q.; Emrick, T.; Russell, T. P. "Self-Corralling" Nanorods under an Applied Electric Field. *Nano Lett.* **2006**, *6*, 2066–2069.
9. Ryan, K. M.; Mastroianni, A.; Stancil, K. A.; Liu, H.; Alivisatos, A. P. Electric-Field-Assisted Assembly of Perpendicularly Oriented Nanorod Superlattices. *Nano Lett.* **2006**, *6*, 1479–1482.
10. Ahmed, S.; Ryan, K. M. Centimetre Scale Assembly of Verically Aligned and Close Packed Semiconductor Nanorods from Solution. *Chem. Commun.* **2009**, 6421–6423.
11. Ding, T.; Song, K.; Clays, K.; Tung, C.-H. Controlled Directionality of Ellipsoids in Monolayer and Multilayer Colloidal Crystals. *Langmuir* **2010**, *26*, 11544–11549.
12. Liu, Q.; Cui, Y.; Gardner, D.; Li, X.; He, S.; Smalyukh, I. I. Self-Alignment of Plasmonic Gold Nanorods in Reconfigurable Anisotropic Fluids for Tunable Bulk Metamaterial Applications. *Nano Lett.* **2010**, *10*, 1347–1353.
13. Goyal, A.; Liu, S.; Iqbal, Z.; Fetter, L. A.; Farrow, R. C. Directed Self-Assembly of Individually Aligned Carbon Nanotubes. *J. Vac. Sci. Technol., B* **2008**, *26*, 2524–2528.
14. Beardslee, J. A.; Sadtler, B.; Lewis, N. S. Magnetic Field Alignment of Randomly Oriented, High Aspect Ratio Silicon Microwires into Vertically Oriented Arrays. *ACS Nano* **2012**, *6*, 10303–10310.
15. Singh, A.; English, N. J.; Ryan, K. M. Highly Ordered Nanorod Assemblies Extending over Device Scale Areas and in Controlled Multilayers by Electrophoretic Deposition. *J. Phys. Chem. B* **2012**, 10.1021/jp305184n.
16. O'Sullivan, C.; Ahmed, S.; Ryan, K. M. Gold Tip Formation on Perpendicularly Aligned Semiconductor Nanorod Assemblies. *J. Mater. Chem.* **2008**, *18*, 5218–5222.
17. Kelly, D.; Singh, A.; Barrett, C. A.; O'Sullivan, C.; Coughlan, C.; Laffir, F. R.; O'Dwyer, C.; Ryan, K. M. A Facile Spin-Cast Route for Cation Exchange of Multilayer Perpendicularly-Aligned Nanorod Assemblies. *Nanoscale* **2011**, *3*, 4580–4583.
18. Mittal, M.; Furst, E. M. Electric Field-Directed Convective Assembly of Ellipsoidal Colloidal Particles To Create Optically and Mechanically Anisotropic Thin Films. *Adv. Funct. Mater.* **2009**, *19*, 3271–3278.
19. Forster, J. D.; Park, J.-G.; Mittal, M.; Noh, H.; Schreck, C. F.; O'Hern, C. S.; Cao, H.; Furst, E. M.; Dufresne, E. R. Assembly of Optical-Scale Dumbbells into Dense Photonic Crystals. *ACS Nano* **2011**, *5*, 6695–6700.
20. Talapin, D. V.; Shevchenko, E. V.; Murray, C. B.; Kornowski, A.; Förster, S.; Weller, H. CdSe and CdSe/CdS Nanorod Solids. *J. Am. Chem. Soc.* **2004**, *126*, 12984–12988.
21. Yella, A.; Tahir, M. N.; Meuer, S.; Zentel, R.; Berger, R.; Panthöfer, M.; Tremel, W. Synthesis, Characterization, and Hierarchical Organization of Tungsten Oxide Nanorods: Spreading Driven by Marangoni Flow. *J. Am. Chem. Soc.* **2009**, *131*, 17566–17575.
22. Zhang, X.; Iame, T. Perpendicular Superlattice Growth of Hydrophobic Gold Nanorods on Patterned Silicon Substrates *via* Evaporation-Induced Self-Assembling. *J. Phys. Chem. C* **2009**, *113*, 5947–5951.
23. Deng, T.; Cournoyer, J. R.; Schermerhorn, J. H.; Balch, J.; Du, Y.; Blohm, M. L. Generation and Assembly of Spheroid-like Particles. *J. Am. Chem. Soc.* **2008**, *130*, 14396–14397.
24. Ahmed, S.; Ryan, K. M. Self-Assembly of Vertically Aligned Nanorod Supercrystals Using Highly Oriented Pyrolytic Graphite. *Nano Lett.* **2007**, *7*, 2480–2485.
25. Carbone, L.; Nobile, C.; De Giorgi, M.; Della Sala, F.; Morello, G.; Pompa, P.; Hytch, M.; Snoeck, E.; Fiore, A.; Franchini, I. R.; *et al.* Synthesis and Micrometer-Scale Assembly of Colloidal CdSe/CdS Nanorods Prepared by a Seeded Growth Approach. *Nano Lett.* **2007**, *7*, 2942–2950.
26. Modestino, M. A.; Chan, E. R.; Hexemer, A.; Urban, J. J.; Segalman, R. A. Controlling Nanorod Self-Assembly

in Polymer Thin Films. *Macromolecules* **2011**, *44*, 7364–7371.
27. Rivest, J. B.; Swisher, S. L.; Fong, L.-K.; Zheng, H.; Alivisatos, A. P. Assembled Monolayer Nanorod Heterojunctions. *ACS Nano* **2011**, *5*, 3811–3816.
28. Zanella, M.; Gomes, R.; Povia, M.; Giannini, C.; Zhang, Y.; Riskin, A.; Van Bael, M.; Hens, Z.; Manna, L. Self-Assembled Multilayers of Vertically Aligned Semiconductor Nanorods on Device-Scale Areas. *Adv. Mater.* **2011**, *23*, 2205–2209.
29. Singh, A.; Gunning, R. D.; Ahmed, S.; Barrett, C. A.; English, N. J.; Garate, J.-A.; Ryan, K. M. Controlled Semiconductor Nanorod Assembly from Solution: Influence of Concentration, Charge and Solvent Nature. *J. Mater. Chem.* **2012**, *22*, 1562–1569.
30. Baker, J. L.; Widmer-Cooper, A.; Toney, M. F.; Geissler, P. L.; Alivisatos, A. P. Device-Scale Perpendicular Alignment of Colloidal Nanorods. *Nano Lett.* **2010**, *10*, 195–201.
31. Mittal, M.; Niles, R. K.; Furst, E. M. Flow-Directed Assembly of Nanostructured Thin Films from Suspensions of Anisotropic Titania Particles. *Nanoscale* **2010**, *2*, 2237–2243.
32. Barry, E.; Dogic, Z. Entropy Driven Self-Assembly of Nonamphiphilic Colloidal Membranes. *Proc. Natl. Acad. Sci. U.S.A.* **2010**, *107*, 10348–10353.
33. Kang, C.-C.; Lai, C.-W.; Peng, H.-C.; Shyue, J.-J.; Chou, P.-T. 2D Self-Bundled CdS Nanorods with Micrometer Dimension in the Absence of an External Directing Process. *ACS Nano* **2008**, *2*, 750–756.
34. Daranov, D.; Fiore, A.; van Huis, M.; Giannini, C.; Falqui, A.; Lafont, U.; Zandbergen, H.; Zanella, M.; Cingolani, R.; Manna, L. Assembly of Colloidal Semiconductor Nanorods in Solution by Depletion Attraction. *Nano Lett.* **2010**, *10*, 743–749.
35. Zhao, N.; Liu, K.; Greener, J.; Nie, Z.; Kumacheva, E. Close-Packed Superlattices of Side-by-Side Assembled Au-CdSe Nanorods. *Nano Lett.* **2009**, *9*, 3077–3081.
36. Guerrero-Martínez, A.; Pérez-Juste, J.; Carbó-Argibay, E.; Tardajos, G.; Liz-Marzán, L. M. Gemini-Surfactant-Directed Self-Assembly of Monodisperse Gold Nanorods into Standing Superlattices. *Angew. Chem.* **2009**, *121*, 9648–9652.
37. Singh, A.; Gunning, R. D.; Sanyal, A.; Ryan, K. M. Directing Semiconductor Nanorod Assembly into 1D or 2D Supercrystals by Altering the Surface Charge. *Chem. Commun.* **2010**, *46*, 7193–7195.
38. Hung, A. M.; Konopliv, N. A.; Cha, J. N. Solvent-Based Assembly of CdSe Nanorods in Solution. *Langmuir* **2011**, *27*, 12322–12328.
39. Zanella, M.; Bertoni, G.; Franchini, I. R.; Brescia, R.; Baranov, D.; Manna, L. Assembly of Shape-Controlled Nanocrystals by Depletion Attraction. *Chem. Commun.* **2011**, *47*, 203–205.
40. Ciszek, J. W.; Huang, L.; Wang, Y.; Mirkin, C. A. Kinetically Controlled, Shape-Directed Assembly of Nanorods. *Small* **2008**, *4*, 206–210.
41. Park, S.; Lim, J.-H.; Chung, S.-W.; Mirkin, C. A. Self-Assembly of Mesoscopic Metal-Polymer Amphiphiles. *Science* **2004**, *303*, 348–351.
42. Kuk Lim, J.; Ciszek, J. W.; Huo, F.; Jang, J.-W.; Hwang, S.; Mirkin, C. A. Actuation of Self-Assembled Two-Component Rodlike Nanostructures. *Nano Lett.* **2008**, *8*, 4441–4445.
43. Ciszek, J. W.; Huang, L.; Tsonchev, S.; Wang, Y.; Shull, K. R.; Ratner, M. A.; Schatz, G. C.; Mirkin, C. A. Assembly of Nanorods into Designer Superstructures: The Role of Templating, Capillary Forces, Adhesion, and Polymer Hydration. *ACS Nano* **2010**, *4*, 259–266.
44. Ou, F. S.; Shaijumon, M. M.; Ajayan, P. M. Controlled Manipulation of Giant Hybrid Inorganic Nanowire Assemblies. *Nano Lett.* **2008**, *8*, 1853–1857.
45. Duran, H.; Hartmann-Azanza, B.; Steinhart, M.; Gehrig, D.; Laquai, F.; Feng, X.; Müllen, K.; Butt, H.-J.; Floudas, G. Arrays of Aligned Supramolecular Wires by Macroscopic Orientation of Columnar Discotic Mesophases. *ACS Nano* **2012**, *6*, 9359–9365.
46. Kelzenberg, M. D.; Boettcher, S. W.; Petykiewicz, J. A.; Turner-Evans, D. B.; Putnam, M. C.; Warren, E. L.; Spurgeon, J. M.; Briggs, R. M.; Lewis, N. S.; Atwater, H. A. Enhanced Absorption and Carrier Collection in Si Wire Arrays for Photovoltaic Applications. *Nat. Mater.* **2010**, *9*, 239–244.
47. Fan, Z.; Razavi, H.; Do, J.-W.; Moriwaki, A.; Ergen, O.; Chueh, Y.-L.; Leu, P. W.; Ho, J. C.; Takahashi, T.; Reichertz, L. A.; *et al.* Three-Dimensional Nanopillar-Array Photovoltaics on Low-Cost and Flexible Substrates. *Nat. Mater.* **2009**, *8*, 648–653.
48. Kapadia, R.; Fan, Z.; Takei, K.; Javey, A. Nanopillar Photovoltaics: Materials, Processes, and Devices. *Nano Energy* **2011**, *1*, 132–144.
49. Triplett, D. A.; Quimby, L. M.; Smith, B. D.; Rodríguez, D. H.; St. Angelo, S. K.; González, P.; Keating, C. D.; Fichthorn, K. A. Assembly of Gold Nanowires by Sedimentation from Suspension: Experiments and Simulation. *J. Phys. Chem. C* **2010**, *114*, 7346–7355.
50. Smith, B. D.; Kirby, D. J.; Keating, C. D. Vertical Arrays of Anisotropic Particles by Gravity-Driven Self-Assembly. *Small* **2011**, *7*, 781–787.
51. Nicewarner-Peña, S. R.; Freeman, R. G.; Reiss, B. D.; He, L.; Peña, D. J.; Walton, I. D.; Cromer, R.; Keating, C. D.; Natan, M. J. Submicrometer Metallic Barcodes. *Science* **2001**, *294*, 137–141.
52. Keating, C. D.; Natan, M. J. Striped Metal Nanowires as Building Blocks and Optical Tags. *Adv. Mater.* **2003**, *15*, 451–454.
53. Almalawi, D.; Liu, C. Z.; Moskovits, M. Nanowires Formed in Anodic Oxide Nanotemplates. *J. Mater. Res.* **1994**, *7*, 1075–1087.
54. Hulteen, J. C.; Martin, C. R. A General Template-Based Method for the Preparation of Nanomaterials. *J. Mater. Chem.* **1997**, *7*, 1075–1087.
55. Sioss, J. A.; Keating, C. D. Batch Preparation of Linear Au and Ag Nanoparticle Chains *via* Wet Chemistry. *Nano Lett.* **2005**, *5*, 1779–1783.
56. Brinker, C. J.; Scherer, G. W. *Sol–Gel Science: The Physics and Chemistry of Sol–Gel Processing*; Academic Press, Inc.: Boston, MA, 1990.
57. Vaidya, S.; Thaplyal, P.; Ganguli, A. K. Enhanced Functionalization of Mn_2O_3@SiO_2 Core–Shell Nanostructures. *Nanoscale Res. Lett.* **2011**, *6*, 169.
58. Ryu, D. H.; Kim, S. C.; Koo, S. M.; Kim, D. P. Deposition of Titania Nanoparticles on Spherical Silica. *J. Sol–Gel Sci. Technol.* **2003**, *26*, 489–493.
59. Caruso, F.; Schüler, C. Enzyme Multilayers on Colloid Particles: Assembly, Stability, and Enzymatic Activity. *Langmuir* **2000**, *16*, 9595–9603.
60. Shchukina, E. M.; Shchukin, D. G. LbL Coated Microcapsules for Delivering Lipid-Based Drugs. *Adv. Drug Delivery Rev.* **2011**, *63*, 837–846.
61. Vergaro, V.; Scarlino, F.; Bellomo, C.; Rinaldi, R.; Vergara, D.; Maffia, M.; Baldassarre, F.; Giannelli, G.; Zhang, X.; Lvov, Y. M.; *et al.* Drug-Loaded Polyelectrolyte Microcapsules for Sustained Targeting of Cancer Cells. *Adv. Drug Delivery Rev.* **2011**, *63*, 847–864.
62. Dean, S. L.; Stapleton, J. J.; Keating, C. D. Organically Modified Silicas on Metal Nanowires. *Langmuir* **2010**, *26*, 14681–14870.
63. Mackenzie, J. D.; Bescher, E. P. Chemical Routes in the Synthesis of Nanomaterials Using the Sol–Gel Process. *Acc. Chem. Res.* **2007**, *40*, 810–818.
64. Walcarius, A.; Collinson, M. M. Analytical Chemistry with Silica Sol–Gels: Traditional Routes to New Materials for Chemical Analysis. *Annu. Rev. Anal. Chem.* **2009**, *2*, 121–143.
65. Hillier, A. C.; Kim, S.; Bard, A. J. Measurement of Double-Layer Forces at the Electrode/Electrolyte Interface Using the Atomic Force Microscope: Potential and Anion Dependent Interactions. *J. Phys. Chem.* **1996**, *100*, 18808–18817.
66. Bargeman, D.; van Voorst Vader, F. van der Waals Forces between Immersed Particles. *J. Electroanal. Chem. Interfacial Electrochem.* **1972**, *37*, 45–52.